THE JOURNAL OF PHYSICAL CHEMISTRY C
A JOURNAL OF THE AMERICAN CHEMICAL SOCIETY

pubs.acs.org/JPCC

Article

On the Mechanism of the Oxygen Reduction Reaction on Au(poly) in Aqueous Alkaline Electrolytes: A Critical Reassessment

Jonathan R. Strobl and Daniel Scherson*

Cite This: *J. Phys. Chem. C* 2021, 125, 13862−13870

Read Online

ACCESS | Metrics & More | Article Recommendations

ABSTRACT: A mechanism is herein proposed for the reduction of oxygen on polycrystalline Au in 0.1 M NaOH + 0.9 M $NaClO_4$ aqueous electrolytes, that assumes, in agreement with theoretical arguments put forward rather recently by Ignaczaket al.. [*Nano Energy* **2016** *26* 558−564], formation of solution-phase superoxide, O_2^-, as the initial, rate-determining step, followed by a reversible (Nernstian) one-electron reduction to yield solution-phase peroxide, HO_2^-(aq), and not by a second-order dismutation of adsorbed O_2^-, as has been postulated by other authors. Also considered in this model is the direct reduction of HO_2^-(aq) and O_2(aq) to generate OH^-(aq). A detailed mathematical analysis of data collected with a rotating ring-disk electrode in O_2-saturated and Ar-purged HO_2^-(aq)-containing solutions made it possible to determine a unique set of kinetic rate constants for the various steps in the proposed mechanism over a wide potential range.

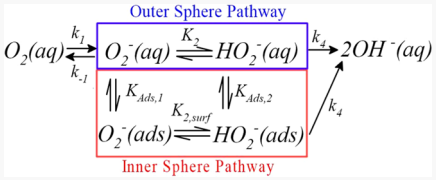

INTRODUCTION

Despite decades of research, questions still remain unanswered regarding critical aspects of the oxygen reduction reaction (ORR) in aqueous electrolytes on a growing number of electrode materials, including polycrystalline and single crystal metals[1,2] and alloys, and functionalized carbon surfaces.[3] Decades ago, Zurilla et al.[4] examined the ORR on polycrystalline gold, Au(poly), in alkaline solutions, using rotating ring-disk electrode (RRDE) techniques. According to these authors, the experimental evidence collected was consistent with a mechanism involving an initial one-electron transfer to yield adsorbed superoxide ion, O_2^-(ads), which, subsequently, undergoes heterogeneous dismutation generating solution-phase peroxide, HO_2^-(aq) and O_2(aq). The same mechanism was later invoked by Adzić et al.[5] for the ORR on Au(100), a surface that displayed extraordinary activity compared to other low index faces of Au. A few years later,[6] the Adzić group proposed a complex, albeit general scheme for the ORR involving seven different adsorbed species, either produced or consumed by one-electron transfer steps, two heterogeneous dismutation reactions, and a single solution-phase intermediate, namely, HO_2^-(aq). Although consensus has been reached among most researchers in this area that the first and rate-determining step (RDS) of the ORR in alkaline media on many electrode materials is a one-electron transfer to yield superoxide ion, O_2^-, whether this species remains in solution or undergoes adsorption on the electrode may still be regarded as a matter of debate. In particular, in a rather recent publication, Ignaczak et al.[7] put forward theoretical arguments that support the view that the initial RDS is actually of the outer-sphere type, generating a solvated O_2^- species, i.e., $O_2(aq) + e^- \underset{k_{-1}}{\overset{k_1}{\rightleftarrows}} O_2^-(aq)$. Moreover, quantum mechanical calculations reported by these authors provided strong evidence that the RDS is followed by yet another outer-sphere one-electron transfer to yield solvated peroxide ion, namely, $O_2^-(aq) + e^- + H_2O \underset{k_{-2}}{\overset{k_2}{\rightleftarrows}} HO_2^-(aq) + OH^-(aq)$, which, assuming six water molecules in the solvation sphere, yielded a barrier height of 0.06 eV. This value is low enough for the process to proceed very fast in both directions, and, thus, consistent with the experimentally observed onset potential observed on metals, such as Au and Ag.

This contribution reexamines the ORR on Au(poly) in 0.1 M NaOH + 0.9 M $NaClO_4$ aqueous solutions using RRDE techniques. Although our data are consistent with the one-electron reduction of O_2(aq) as the ORR rate-determining step, we found no evidence for a second-order heterogeneous dismutation of O_2^-(ads). In fact, O_2^-(aq) seems to undergo a fast, subsequent one-electron reduction to yield HO_2^-(aq), as proposed by Ignaczak et al.,[7] which can then be reduced to produce solution-phase hydroxyl ion, OH^-(aq). Additional experiments carried out in N_2-purged, HO_2^-(aq)-containing solutions indicated that HO_2^-(aq) oxidation proceeds via first-, and not half-order kinetics, as previously reported in the literature.[4,5] Also considered in the ORR mechanism proposed herein is the possibility of a direct 4e$^-$ reduction of O_2(aq) to yield solution-phase hydroxyl ions. A quantitative analysis of all

Received: March 25, 2021
Revised: May 19, 2021
Published: June 17, 2021

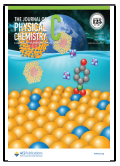

https://doi.org/10.1021/acs.jpcc.1c02683
J. Phys. Chem. C 2021, 125, 13862−13870

of the experimental data we collected yielded potential-dependent values for the rate constants of the four redox reactions involved, which were found to be independent of the concentration of HO_2^-(aq). Also consistent with the experimental data was a mechanism in which the reduction of O_2^- proceeds via an inner-sphere pathway involving adsorbed species in equilibrium with their solution-phase counterparts. However, a critical assessment of the published spectroscopic data was not found to provide solid evidence for the presence of such adsorbed species.

METHODS

Solutions of 0.1 M NaOH in 0.9 M $NaClO_4$ were prepared with $HClO_4$ (Sigma-Aldrich, 67−72%, Traceselect) and NaOH (Honeywell, Semiconductor Grade, 99.99% metal basis) mixed in appropriate quantities, using ultrapure water from a Barnstead NANOpure DIamond water purification system. For the ORR measurements, oxygen (Airgas, 99.999%) was bubbled through the electrolyte for a minimum of 10 min before each experiment, or until the O_2 reduction currents became time-independent. Additional experiments were performed in nitrogen (Airgas, 99.998%)-purged hydrogen peroxide (Fisher, 30%, Certified ACS) solutions. A Pine ChangeDisk AuIAu RRDE rotated with a Pine Analytical Rotator driven by a Pine MSRX Speed Controller was used as the working electrode. The geometric area of the Au disk was 0.196 cm^2. A graphite rod was used as a counter electrode, and a home-made hydrogen bubble reversible hydrogen electrode (RHE)[8] was used as a reference electrode. All cell components were made of glass or Teflon and cleaned by soaking overnight in piranha solution (10:1 concentrated H_2SO_4 (Fisher, Certified ACS Plus) to 30% aqueous H_2O_2) followed by alternatively rinsing and boiling in ultrapure water (4−5 times each). Piranha solution is highly corrosive and oxidizing and, thus, care must be exercised during its preparation and handling. The thiol-modified Au ring electrode was prepared by removing the Au disk from the AuIAu RRDE and replacing it with a Teflon insert. This assembly was then immersed into a 10 mM solution of 3-mercapto-1-propanol (3M1P, Aldrich, 95%) in ethanol (Decon Laboratories Inc., 200 proof) for a minimum of 12 h. Following rinsing with ultrapure water, the Teflon insert was replaced by the (bare) Au disk. All electrochemical experiments were carried out with a Pine RDE 3 potentiostat.

Mechanistic Considerations. The reaction mechanism considered herein, shown schematically in eqs 1−4, was proposed by Ignaczak et al.[7] based on their theoretical calculations. As indicated, the first, and rate-determining step, eq 1, involves an outer-sphere one-electron transfer to yield solution-phase superoxide ion, O_2^-(aq), which is then followed by a fast and reversible one-electron transfer to generate HO_2^-(aq), eq 2. Also included in this scheme are two additional highly irreversible reactions, i.e., the four-electron reduction of O_2, eq 3, and the two-electron reduction of HO_2^-(aq), eq 4, which yield, in both cases, OH^-(aq) as the product.

$$O_2(aq) + e^- \underset{k_{-1}}{\overset{k_1}{\rightleftarrows}} O_2^-(aq) \tag{1}$$

$$O_2^-(aq) + e^- + H_2O \underset{k_{-2}}{\overset{k_2}{\rightleftarrows}} HO_2^-(aq) + OH^-(aq) \tag{2}$$

$$O_2(aq) + 4e^- + 2H_2O \xrightarrow{k_3} 4OH^-(aq) \tag{3}$$

$$HO_2^-(aq) + 2e^- + H_2O \xrightarrow{k_4} 3OH^-(aq) \tag{4}$$

This scheme neglects the possible homogeneous dismutation of O_2^-(aq), as its rate, under the conditions selected for the experiments herein described, is too small for this reaction to proceed to any significant extent during the transit time from the disk to the ring.[9] It should be emphasized that both solution-phase intermediates, O_2^-(aq), and HO_2^-(aq), would be oxidized on a conventional Au ring; however, functionalization of Au with a monolayer of 3M1P imparts the electrode extraordinary specificity for O_2^-(aq), oxidation, while remaining impervious to the presence of HO_2^-(aq),[9,10] as illustrated in our recent studies of the ORR on glassy carbon electrodes in our laboratories.

If one assumes that the superoxide intermediate is strictly in solution, i.e., O_2^-(aq), reactions in eqs 1 and 2 above represent a special case of a more general mechanism analyzed in detail by Bard and Faulkner,[11] namely

$$O + n'e^- \rightleftarrows O' \tag{5}$$

$$O' + e^- \underset{k_b}{\overset{k_f}{\rightleftarrows}} R' \tag{6}$$

$$R' + n''e^- \rightleftarrows R \tag{7}$$

where, in our case, there is no step (5), i.e., $n' = 0$, eq 6 is the RDS, and eq 7 is a following kinetically reversible one-electron transfer, $n'' = 1$, assumed to be in equilibrium. Equations 6 and 7 are, respectively, analogous to the processes in eqs 1and 2 above. The analysis outlined here is applicable to the case where O_2^- is only present in solution. Under these conditions, the current associated with this scheme may be shown to be given by[11]

$$i = FAnk^0_{RDS}[C_{O'}(0, t)e^{-\alpha f(E-E^{0'}_{RDS})} - C_{R'}(0, t)e^{(1-\alpha)f(E-E^{0'}_{RDS})}] \tag{8}$$

where $C_X(0, t)$ is the concentration of X = O′ and R′ in a region immediately adjacent to the electrode surface at a time t, and k^0_{RDS}, α, and $E^{0'}_{RDS}$ are, respectively, the standard kinetic rate constant, transfer coefficient, and formal redox potential of the RDS, $f = F/RT$, and $n = n' + n'' + 1$. As shown by Bard and Faulkner, eq 8 can be expressed in terms of the concentrations of O and R, namely

$$i = FAnk^0_{RDS}[C_O(0, t)e^{-n'f(E-E^{0'}_{pre})}e^{-\alpha f(E-E^{0'}_{RDS})} - C_R(0, t)e^{n''f(E-E^{0'}_{post})}e^{(1-\alpha)f(E-E^{0'}_{RDS})}] \tag{9}$$

The symbols $E^{0'}_{pre}$ and $E^{0'}_{post}$ in this equation represent the formal redox potentials of the reactions that precede, pre, and follow, post, the RDS, respectively. When applied to the mechanism for the ORR herein proposed, i.e., eqs 1 and 2 above, i.e., $n' = 0$, $n'' = 1$, $n = 2$; hence, eq 8 can be written as

$$i = -2FAk^0_1([O_2]_S e^{-\alpha f(E-E^{0'}_1)} - [O_2^-]_S e^{(1-\alpha)f(E-E^{0'}_1)}) \tag{10}$$

where $E^{0'}_{RDS}$ in eq 9 is now defined as $E^{0'}_1$, and, in anticipation of the data analysis to follow, $C_o(0, t)$ and $C_R(0, t)$ have been replaced by their specific steady-state equivalents at the electrode surface, $[O_2]_S$ and $[O_2^-]_S$, respectively. In addition, we have inverted the sign of the currents in eq 10 to conform to the standard notation in physical electrochemistry. As our

https://doi.org/10.1021/acs.jpcc.1c02683
J. Phys. Chem. C 2021, 125, 13862−13870

Table 1. Disk Current and Mass Balance Equations for the Reduction of Dioxygen and Hydrogen Peroxide in Alkaline Solution

$$i_{\text{disk},O_2} = 2FA\{(k_{-12} - k_4)[HO_2^-]_{S,O_2} - (2k_3 + k_{12})[O_2]_{S,O_2}\}$$

$$-\frac{D_{O_2}([O_2]_{S,O_2} - [O_2]_B)}{\delta_{O_2}} - (k_3 + k_{12})[O_2]_{S,O_2} + k_{-12}[HO_2^-]_{S,O_2} = 0$$

$$-\frac{D_{HO_2^-}[HO_2^-]_{S,O_2}}{\delta_{HO_2^-}} + k_{12}[O_2]_{S,O_2} - (k_4 + k_{-12})[HO_2^-]_{S,O_2} = 0$$

$$k_{12} = k^0_{\text{eff},12}e^{-\alpha f(E - E^{0'}_{12})}$$

$$i_{\text{disk},HO_2^-} = 2FA\{(k_{-12} - k_4)[HO_2^-]_{S,HO_2^-} - (2k_3 + k_{12})[O_2]_{S,HO_2^-}\}$$

$$-\frac{D_{HO_2^-}([HO_2^-]_{S,HO_2^-} - [HO_2^-]_B)}{\delta_{HO_2^-}} + k_{12}[O_2]_{S,HO_2^-} - (k_4 + k_{-12})[HO_2^-]_{S,HO_2^-} = 0$$

$$-\frac{D_{O_2}[O_2]_{S,HO_2^-}}{\delta_{O_2}} - (k_3 + k_{12})[O_2]_{S,HO_2^-} + k_{-12}[HO_2^-]_{S,HO_2^-} = 0$$

$$k_{-12} = k^0_{\text{eff},12}e^{(2-\alpha)f(E - E^{0'}_{12})}$$

Table 2. Algebraic Expressions for the Four Rate Constants Associated with the Proposed ORR Mechanism

$$k_3 = \frac{D_{O_2}(2FAD_{HO_2^-}[HO_2^-]_B[HO_2^-]_{S,O_2} - \delta_{HO_2^-}\{[HO_2^-]_{S,O_2}i_{\text{disk},HO_2^-} - [HO_2^-]_{S,HO_2^-}i_{\text{disk},O_2}\})}{2FAD_{HO_2^-}[HO_2^-]_B[HO_2^-]_{S,O_2}\delta_{O_2} - 4FAD_{O_2}[O_2]_B[HO_2^-]_{S,HO_2^-}\delta_{HO_2^-} + ([HO_2^-]_{S,O_2}i_{\text{disk},HO_2^-} - [HO_2^-]_{S,HO_2^-}i_{\text{disk},O_2})\delta_{HO_2^-}\delta_{O_2}}$$

$$k_{12} = -\frac{4FAD_{HO_2^-}D_{O_2}[HO_2^-]_B[HO_2^-]_{S,O_2}}{2FAD_{HO_2^-}[HO_2^-]_B[HO_2^-]_{S,O_2}\delta_{O_2} - 4FAD_{O_2}[O_2]_B[HO_2^-]_{S,HO_2^-}\delta_{HO_2^-} + ([HO_2^-]_{S,O_2}i_{\text{disk},HO_2^-} - [HO_2^-]_{S,HO_2^-}i_{\text{disk},O_2})\delta_{HO_2^-}\delta_{O_2}}$$

$$k_{-12} = \frac{-D_{O_2}[O_2]_B i_{\text{disk},HO_2^-}\delta_{HO_2^-} - 2FAD_{HO_2^-}D_{O_2}[O_2]_B([HO_2^-]_B - [HO_2^-]_{S,HO_2^-})}{2FAD_{HO_2^-}[HO_2^-]_B[HO_2^-]_{S,O_2}\delta_{O_2} - 4FAD_{O_2}[O_2]_B[HO_2^-]_{S,HO_2^-}\delta_{HO_2^-} + ([HO_2^-]_{S,O_2}i_{\text{disk},HO_2^-} - [HO_2^-]_{S,HO_2^-}i_{\text{disk},O_2})\delta_{HO_2^-}\delta_{O_2}}$$

$$k_4 = -\frac{D_{HO_2^-}[HO_2^-]_B i_{\text{disk},O_2}\delta_{O_2} - D_{O_2}[O_2]_B i_{\text{disk},HO_2^-}\delta_{HO_2^-} + D_{HO_2^-}\delta_{O_2}\{[HO_2^-]_{S,O_2}i_{\text{disk},HO_2^-} - [HO_2^-]_{S,HO_2^-}i_{\text{disk},O_2}\} + 2FAD_{HO_2^-}D_{O_2}[O_2]_B([HO_2^-]_B - [HO_2^-]_{S,HO_2^-})}{2FAD_{HO_2^-}[HO_2^-]_B[HO_2^-]_{S,O_2}\delta_{O_2} - 4FAD_{O_2}[O_2]_B[HO_2^-]_{S,HO_2^-}\delta_{HO_2^-} + ([HO_2^-]_{S,O_2}i_{\text{disk},HO_2^-} - [HO_2^-]_{S,HO_2^-}i_{\text{disk},O_2})\delta_{HO_2^-}\delta_{O_2}}$$

$$[HO_2^-]_{S,O_2} = \frac{i_{\text{ring},O_2}\delta_{HO_2^-}}{2FAND_{HO_2^-}} \qquad [HO_2^-]_{S,HO_2^-} = \frac{(i_{\text{ring},HO_2^-} - i^{E_{\text{disk}}=1.15\text{ V}}_{\text{ring},HO_2^-})\delta_{HO_2^-}}{2FAND_{HO_2^-}}$$

mechanism prescribes, the O_2^-(aq)|HO_2^-(aq) redox couple (see eq 2) is very fast; hence, the potential can be related to their interfacial activities via the Nernst equation, i.e., $E = E_2^0 - \frac{1}{f}\ln\left(\frac{a_{HO_2^-,s} \times a_{OH^-,s}}{a_{O_2^-,s}}\right)$, which, to a very good degree of approximation under the conditions of our experiments, can be expressed as $E = E_2^{0'} - \frac{1}{f}\ln\frac{[HO_2^-]_S}{[O_2^-]_S}$, where $E_2^{0'} = E_2^0 - \frac{1}{f}\ln a_{OH^-,S} - \frac{1}{f}\ln\frac{\gamma^S_{HO_2^-}}{\gamma^S_{O_2^-}}$ is the formal potential of the redox couple.[12] On this basis, eq 10 can be shown to be given by

$$i = -2Fk_1^0([O_2]_S e^{-\alpha f(E - E_1^{0'})} - [HO_2^-]_S e^{f(E - E_2^{0'})}e^{(1-\alpha)f(E - E_1^{0'})}) \tag{11}$$

which is analogous to eq 9, keeping in mind that $n' = 0$, $n'' = 1$, and $n = 2$. It is interesting to note that the exponentials of the second term in parentheses in eq 11 can be written as $e^{-fE_2^{0'} - (1-\alpha)fE_1^{0'}}e^{(2-\alpha)fE}$. Hence, the oxidation rate constant will scale as $e^{(2-\alpha)fE}$, while the reduction rate constant will scale as $e^{-\alpha fE}$. Clearly, the oxidation rate constant will increase much faster with increasing E than the reduction rate constant will with decreasing E. This clearly illustrates that for a multistep process, such as the one being herein considered, the current potential behavior can seldom be expressed as a conventional Butler–Volmer expression, where the transfer coefficients are α and $(1 - \alpha)$, a fact that has been emphasized by Bard and Faulkner.[11]

A particularly appealing form of eq 11 can be obtained by selecting the formal redox potential of the O_2(aq)|HO_2^-(aq) redox couple, i.e., $\frac{1}{2}(E_1^{0'} + E_2^{0'})$, to be denoted hereafter as $E_{12}^{0'}$, as a reference potential common to both the reduction and oxidation branches, namely

$$i = -2FAk^0_{\text{eff},12}[[O_2]_S e^{-\alpha f(E - E^{0'}_{12})} - [HO_2^-]_S e^{(2-\alpha)f(E - E^{0'}_{12})}]$$
$$= -2FA\{k_{12}[O_2]_S - k_{-12}[HO_2^-]_S\} \tag{12}$$

The term $k^0_{\text{eff},12} = k_1^0 \exp\left\{\alpha f\left(\frac{E_1^{0'} - E_2^{0'}}{2}\right)\right\}$ in this equation represents the unique potential-independent standard rate constant associated with the overall reduction process, which can be used to define potential-dependent rate constants for the reduction of O_2 to HO_2^-, $k_{12} = k^0_{\text{eff},12}e^{-\alpha f(E - E_{12}^{0'})}$, and the oxidation of HO_2^- to O_2, $k_{-12} = k^0_{\text{eff},12}e^{(2-\alpha)f(E - E_{12}^{0'})}$ (see right-hand side in eq 12). As will be shown, the analysis of the experimental data will make it possible to determine the values of both k_{12} and k_{-12}, and thus $k^0_{\text{eff},12}$ and α.

The value of $E_2^{0'}$ can be estimated based on [OH^-] and the standard redox potentials for[13−15]

$$O_2(g) + e^- \rightarrow O_2^-(aq); \qquad E_A^0 = -0.33\text{ V vs SHE} \tag{13}$$

$$O_2(g) + 2e^- + H_2O \rightarrow HO_2^-(aq) + OH^-(aq); \qquad E_B^0 = -0.076\text{ V vs SHE} \tag{14}$$

from which O_2^-(aq) + e^- + H_2O → HO_2^-(aq) + OH^-(aq); E_2^0 = 0.178 V vs SHE.

Hence, for pH 13, E_2^0 = 0.945 V vs RHE. Accounting for the contribution of [OH^-], we can estimate $E_2^{0'}$ = 1.004 V vs RHE, assuming a negligible contribution from activity coefficients. Also of interest is the fact that the standard (not formal) potential for the aqueous oxygen/aqueous superoxide redox couple, listed in the literature, eq 13, is given in terms of the

https://doi.org/10.1021/acs.jpcc.1c02683
J. Phys. Chem. C 2021, 125, 13862−13870

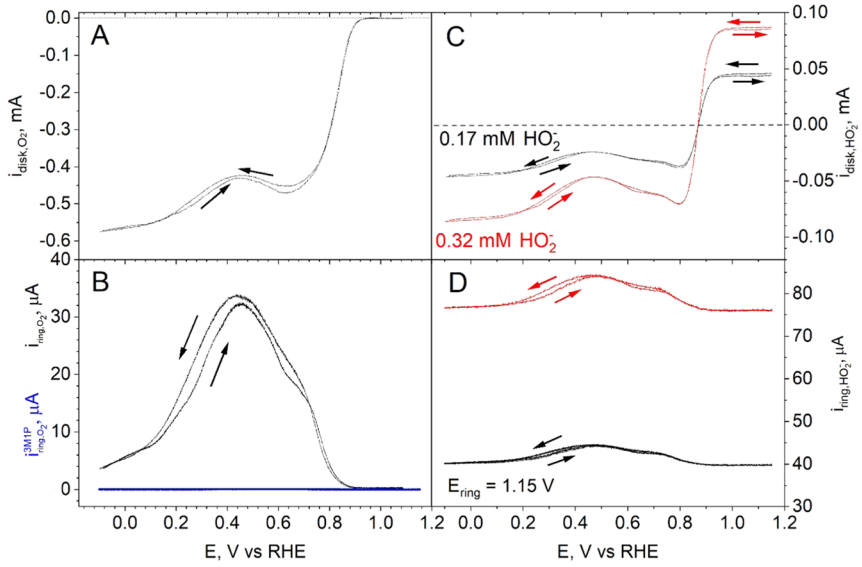

Figure 1. (A) Dynamic polarization curves collected with the Au(poly) disk electrode of a Au(poly)|Au(poly) RRDE at a rotation rate ω = 900 rpm and a scan rate ν = 20 mV/s in O_2-saturated 0.1 M NaOH + 0.9 M $NaClO_4$, where the arrows indicate the direction of the scan. (B) Plots of i_{ring,O_2} collected for E_{ring} = 1.15 V while the curve in (A) was being recorded. The blue curve was collected with a 3M1P-functionalized Au ring polarized at E_{ring} = 0.9 V under otherwise the same conditions. (C) Same as in (A) recorded in N_2-saturated base electrolyte containing 0.17 mM (black curve) or 0.32 mM (red curve) HO_2^-(aq). (D) Plots of i_{ring,HO_2^-} collected with a bare Au ring polarized at E_{ring} = 1.15 V while the data in (C) were being recorded. All of the data were collected at room temperature, i.e., 294.15 K.

activity of O_2 in the gas phase, and not as a solution-phase species. Once corrected for the solvation energy of O_2(gas)[13,14] and converted to our RHE scale, so it is directly applicable to our experimental conditions, the value of the standard potential E_1^0 may be shown to be 0.617 V vs RHE. Finally, the estimate for $E_{12}^{0\prime}$ (assuming the activity coefficients for the ions in question to be the mean activity coefficient for 1 m NaOH reported in the *CRC Handbook of Chemistry and Physics*,[16] i.e., 0.678)) is 0.820 V vs RHE. This is the potential where the anodic and cathodic rate constants of eq 12, k_{12} and k_{-12}, are expected to be equal to one another and to $k_{eff,12}^0$.

It should be emphasized that eq 12 only accounts for contributions to the current derived solely from the reactions in eqs 1 and 2, and, as such, should be added to those associated with the four-electron and two-electron irreversible reductions of O_2(aq) and HO_2^-(aq) (see eqs 3 and 4), to yield the total measured disk current, i_{disk}. Expressions for i_{disk} in O_2-saturated, i_{disk,O_2}, and N_2-purged HO_2^--containing solutions, i_{disk,HO_2^-}, are given in the left and right top entries in Table 1, respectively. Also, directly beneath in this table are the interfacial mass balances of O_2(aq) (left column) and HO_2^-(aq) (right column) in the same two solutions, where $\delta_X = \frac{1.61 D_X^{1/3} \nu^{1/6}}{\omega^{1/2}}$, X = O_2, HO_2^-, represents the thickness of the diffusion boundary layer; D_X is the diffusion coefficient of X; ν is the kinematic viscosity of the solution, and ω is the rotation rate of the electrode in radian/s. The six equations in Table 1 can be combined to yield explicit expressions for the four potential-dependent rate constants, i.e., k_{12}, k_{-12}, k_3, and k_4, in terms of $i_{disk,X}$ and $[HO_2^-]_{S,X}$, X = O_2, HO_2^- (see Table 2), and other known parameters. Therefore, these rate constants can be calculated within the potential range, where i_{disk,O_2}, $[HO_2^-]_{S,O_2}$, i_{disk,HO_2^-}, and $[HO_2^-]_{S,HO_2^-}$ can be measured.

The values of $[HO_2^-]_S$ can be determined from i_{ring,O_2}, the current flowing through the ring polarized at E_{ring} = 1.15 V vs RHE, a potential positive enough for the oxidation of HO_2^-(aq) to proceed under strict diffusion control, i.e., $[HO_2^-]_{S,O_2} = \frac{i_{ring,O_2}\delta_{HO_2^-}}{2FAND_{HO_2^-}}$ whereas those of $[HO_2^-]_{S,HO_2^-}$ can be obtained from a shielding experiment, i.e., $[HO_2^-]_{S,HO_2^-} = \frac{(i_{ring,HO_2^-} - i_{ring,HO_2^-}^{E_{disk}=1.15\ V})\delta_{HO_2^-}}{2FAND_{HO_2^-}}$, where $i_{ring,HO_2^-}^{E_{disk}\ =\ 1.15\ V}$ is the ring current recorded at E_{disk} = 1.15 V.

RESULTS AND DISCUSSION

Figure 1A shows dynamic polarization curves recorded with the Au disk of a Au(poly)|Au(poly) RRDE while scanning at a rate ν = 20 mV/s, at a rotation rate ω = 900 rpm in O_2–saturated 0.1 M NaOH in 0.9 M $NaClO_4$ base electrolyte. The currents recorded with the concentric Au ring electrode polarized at E_{ring} = 1.15 V, i.e., i_{ring,O_2}, while the Au(poly) disk was being scanned, are shown in Figure 1B. The blue curve in this panel was obtained under identical conditions, except that the Au(poly) ring was functionalized with a monolayer of 3M1P, a surface modification that imparts Au(poly) extraordinary specificity toward O_2^-(aq) oxidation,[9,10] and polarized at E_{ring} = 0.90 V. It should be mentioned that for E_{ring} > 0.90 V, the thiol monolayer was found to oxidatively desorb from the electrode surface at increasing rates and, therefore, higher potentials were avoided. The fact that i_{ring,O_2}^{3M1P} was undetectable does not necessarily mean that O_2^-(aq) is not involved in the ORR on Au(poly) under these experimental conditions. In fact, it is possible that O_2^-(aq) undergoes reduction at very high rates, making its concentration too small to be detected. For example, if we assume the reaction in eq 2 to be reversible, i.e., always at equilibrium, the concentration of O_2^-(aq) at the electrode surface, based on the corresponding Nernst equation and the experimentally measured $[HO_2^-]_{S,O_2}$, would be below 0.1 μM in the potential range of interest, generating an i_{ring} of ca. 6 pA, and thus too small to be

https://doi.org/10.1021/acs.jpcc.1c02683
J. Phys. Chem. C 2021, 125, 13862−13870

measured with our current instrumentation. Alternatively, O_2^- may actually be adsorbed and not in solution. In fact, as discussed in a subsequent section, the Butler−Volmer equations that would govern the reaction kinetics would be indistinguishable, regardless of whether O_2^- is in solution or adsorbed, as long as reaction 2 is very fast.

Plots of i_{disk,HO_2^-} and i_{ring,HO_2^-} vs E collected in N_2-purged base electrolyte containing either 0.17 mM (black) or 0.32 mM (red) HO_2^-(aq) are shown in Figure 1C,D. The overall shape of the curves in Figure 1A,C are very similar to those reported by Srejić et al.[17] at the same pH, including the hump maxima at about 0.3 V more negative to the onset of O_2 reduction in (panel A), and that at ca. 0.2 V negative to the onset of HO_2^-(aq) reduction (panel C). Additional small differences in the curves may be ascribed to details in surface preparation, as demonstrated by Srejić et al.[17] and Paleteiro.[18] Note that the values of the limiting currents for the oxidation (E = 1.15 V vs RHE) and reduction (E = −0.1 V vs RHE) of HO_2^-(aq) are not only virtually identical for a given concentration, but the ratios for the two concentrations are in excellent agreement with the relative values of [HO_2^-(aq)] in these two experiments.

As explained above, the values of i_{disk,O_2}, i_{ring,O_2}, i_{disk,HO_2^-}, and i_{ring,HO_2^-} in Figure 1 were then used with the expressions in Table 2 and the parameters listed in Table 3 to generate plots

Table 3. List of Parameters and Their Values

symbol	value	meaning
[OH^-]	0.1 M	concentration of OH^-
N	0.21	collection efficiency of the RRDE assembly
D_{O_2}	1.8 × 10^{-5} cm^2 s^{-1}	diffusion coefficient of O_2(aq)[35]
$D_{HO_2^-}$	1.3 × 10^{-5} cm^2 s^{-1}	diffusion coefficient of HO_2^-(aq)[36]
ω	900 rpm (94 rad s^{-1})	rotation rate of the RRDE
ν	0.01 cm^2 s^{-1}	kinematic viscosity of water
T	294.15 K	absolute temperature
$[O_2]_B$	0.885 mM[1]	bulk concentration of O_2 in O_2-containing solutions
$[HO_2^-]_B$	0.170 or 0.315 mM	bulk concentration of HO_2^- in HO_2^--containing solutions
A	0.196 cm^2	cross-sectional area of the disk electrode

[1]See Appendix B for a detailed determination of $[O_2]_B$ from the experimental data.

of the four rate constants as a function of potential. These are displayed in Figure 2 for data collected in O_2-purged solution and N_2-purged 0.17 mM HO_2^-(aq) (see solid lines) or 0.34 mM HO_2^-(aq) (see dotted lines) solutions. As indicated, both sets yielded virtually identical results, affording strong evidence that the rate constants are independent of the concentration of HO_2^-(aq) in solution, and, thus, consistent with the mechanism for the ORR herein presented.

As predicted by the Butler−Volmer model, k_{-12}, the rate constant for HO_2^-(aq) oxidation (see Table 1), shows a much steeper increase with $E - E_{12}^{0\prime}$ compared to k_{12}, the corresponding rate constant for the 2 e^- reduction of O_2(aq). The potential at which k_{12} and k_{-12} cross, E = 0.818 V, shown more clearly in Figure 3, matches very closely the estimate for the formal potential, $E_{12}^{0\prime}$ = 0.820 V, for each data set, lending strong support to the mechanism herein proposed. As should be evident from the expressions in Table 1, k_{12} and

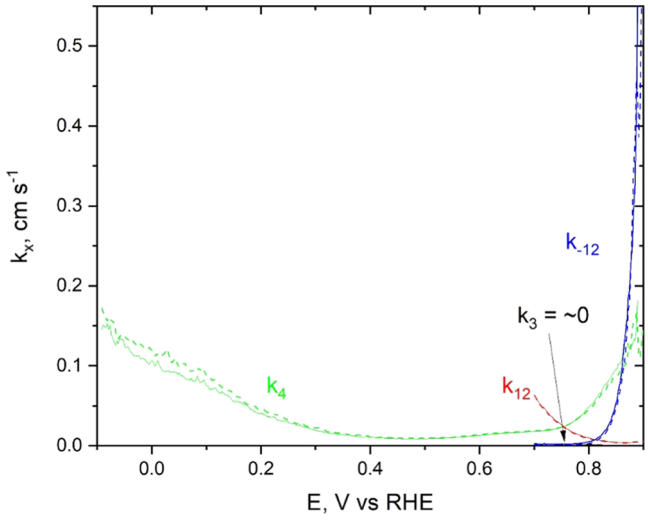

Figure 2. Plots of k_{12} (red), k_{-12} (blue), k_3 (black), and k_4 (green) as a function of potential determined from the expressions in Table 2. The rate constants were calculated using i_{disk} and i_{ring} collected in O_2-saturated solutions, and Ar-purged 0.17 mM HO_2^-(aq) (solid line) or 0.32 mM HO_2^-(aq) (dashed) solutions (see text for details). Note that rate constants are only shown at potentials where the O_2(aq) and HO_2^-(aq) surface concentrations at the disk are greater than 2% of their corresponding bulk concentrations, and i_{disk,O_2} is more negative than −5 μA.

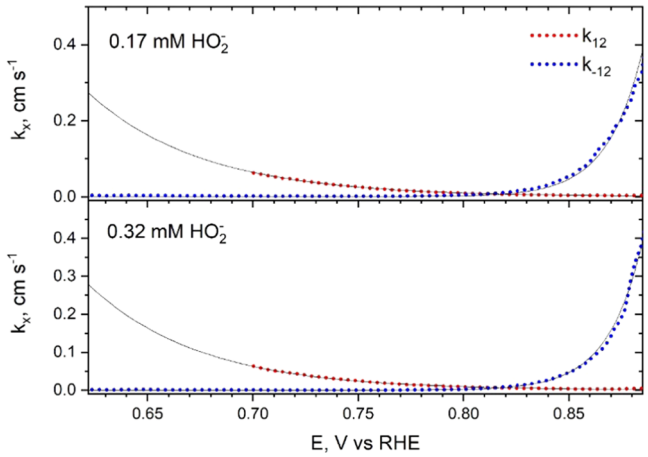

Figure 3. Rate constant data from Figure 2 in an expanded potential region around the crossing point of k_{12} (red) and k_{-12} (blue). The black solid lines represent the best fits assuming the rate constants to be of the form shown in the last row, Table 1.

k_{-12} should both equal $k_{eff,12}^0$ when $E = E_{12}^{0\prime}$. The solid black lines in Figure 3 are the best fits to the experimental data, assuming the rate constants are of the form specified in the last row in Table 1, which yielded values of $k_{eff,12}^0$ and α extracted from the two independent set of experimental results within a few percent of one another (see Table 4), as would be required for the current to be accurately described by eq 12. Moreover, the fact that k_3 is virtually negligible over the potential range examined (see Figure 2) is in agreement with the reports of Wroblowa et al.,[19] who based their conclusions on plots of i_{disk}/i_{ring} vs $\omega^{1/2}$ slopes vs their intercepts (or J−S plots), which yielded for Au in 2 M KOH, a zero intercept, consistent with k_3 = 0. Zurilla et al.[4] found that k_4, the rate constant for HO_2^-(aq) reduction over the range 0.75 V (just negative to

https://doi.org/10.1021/acs.jpcc.1c02683
J. Phys. Chem. C 2021, 125, 13862−13870

Table 4. Best-Fit Values for k_{12} and k_{-12} Assuming the Rate Constants to Be of the Form Specified in the Last Row, Table 1, and $E^{0\prime}_{12}$ = 0.818 V vs RHE

rate constant	$[O_2]_B$ (mM)	$[HO_2^-]_B$ (mM)	$k^0_{eff,12}$ (cm s^{-1})	α
k_{12}	0.885	0.17	0.00721	0.474
	0.885	0.32	0.00681	0.505
k_{-12}	0.885	0.17	0.00715	0.484
	0.885	0.32	0.00659	0.491
average			0.00694 ± 0.00029	0.49 ± 0.01

the onset of the reaction) down to 0.2 V vs H/ β-Pd, was relatively small, i.e., ca. 0.01 cm/s, and displayed hardly any potential dependence. This observation led these authors to conclude that the rate-controlling step, and any step preceding it, did not involve electron transfer. However, as clearly indicated by our results in Figure 2 (see green curve), the rate constant does increase rather markedly as the potential is extended down to negative values. Interestingly, the rate constant also increases for E > 0.7 V vs RHE, an effect also observed for Au(100) which has been ascribed either to enhanced HO_2^-(aq) adsorption with increasing potential,[20] ease of formation of catalytically active OH(ads),[5] or surface reconstruction.[21]

Past work by Zurilla et al.[4] and Adzić et al.[5] reported a reaction order of 1/2 for HO_2^-(aq) during its oxidation at polycrystalline Au and Au(100), respectively. Our own work has revealed a reaction order of 1. To clarify this inconsistency, we attempted to recalculate the reaction orders published by Zurilla et al.[4] and Adzić et al.[5] using their own data. Details regarding our analysis of their data are provided in Appendix A. As shown therein, the reaction orders obtained using digitization methods to extract relevant values from their dynamic polarization curves were found, with only one exception, to deviate significantly from 0.5. We have not been able to determine the source of this discrepancy.

On the Possible Involvements of Adsorbed Species in the ORR in Aqueous Electrolytes. The reaction mechanism considered in the previous section regarded O_2^- generated in the first and rate-determining step, eq 1, as a strictly solution-phase species. However, the experimentally observed kinetics are consistent with any reaction scheme that includes a fast, reversible O_2^-(aq)/HO_2^-(aq) interconversion. In other words, the single reaction in eq 2, assumed to be outer sphere, can instead be reexpressed as a series of fast, reversible reactions which provide a pathway from O_2^-(aq) to HO_2^-(aq), leading to a Butler–Volmer equation of a form indistinguishable from that shown in the previous section, i.e., eq 12. An example of one such mechanism is shown in Scheme 1, which features three fully reversible reactions following the rate-determining step, namely, adsorption of O_2^-, O_2^-(ads)/HO_2^-(ads) interconversion, which itself may be composed of several elementary steps, and desorption of HO_2^-(ads). The adsorption equilibria are thought to play a role, since O_2^-(aq) and HO_2^-(aq) are expected to adsorb at potentials positive of the PZC as numerous anions do.

Scheme 1. Alternate Mechanism for 2 e^- ORR on Au(poly) Surface Involving Adsorbed Intermediates

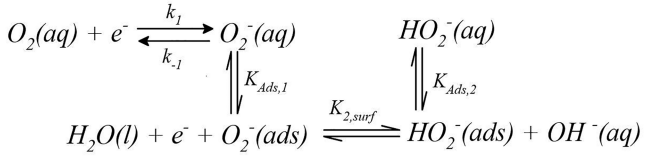

A number of authors have attempted to unveil the nature of the intermediates in the ORR on Au electrodes in aqueous electrolytes using vibrational spectroscopies. A brief summary of the information so far reported, mostly in alkaline solutions, is provided in the next section.

In Situ Vibrational Spectroscopy for the ORR on Au(poly) in Alkaline Solutions. As early as 2005, Shao and Adzić[22] reported in situ potential difference (PD) attenuated total reflection (ATR)-surface-enhanced infrared absorption spectroscopy (SEIRAS) data collected from a Au thin-film electrode in O_2-saturated acidic and alkaline solutions as a function of the applied potential, E. Spectra recorded by these authors in 0.1 M $NaClO_4$ (pH 9, E_{ref} = 0.4 V vs Ag|AgCl) revealed the presence of a band at $\tilde{\nu}$ = 1268 cm^{-1} in the potential range where the ORR was observed, i.e., 0.1 ≤ E ≤ −0.6 V vs Ag|AgCl or 0.322 ≤ E ≤ −0.378 V vs SHE. The integrated intensity, A_{int}, of this feature was found to increase as E shifted in the negative direction reaching a maximum at E = 0.022 V vs SHE and then decreasing gradually at more negative values. Interestingly, this band disappeared upon replacing water by D_2O, leading these authors to assign it to the antisymmetric bending mode of OOH of adsorbed HO_2^-, HO_2^-(ads). Curiously, and in stark contrast to the earlier work of Brooker et al.,[23] Shao and Adzić did not observe any peaks attributable to O_2^-. A few years later, Kim and Gewirth,[24] detected a peak at 1150 cm^{-1} in the in situ surface-enhanced Raman scattering, SERS, spectra (λ_{exc} = 668 nm) collected with a roughened Au electrode in O_2-saturated 0.1 M NaOH over the same potential range, the A_{int} of which increased monotonically as E was shifted negatively. In direct analogy to the earlier work of Hunter-Saphir and Creighton[25] with solid KO_2 and CsO_2 salts, they ascribed this feature to the O–O stretching mode of O_2^-(ads). Note that the corresponding mode for (neutral) dioxygen[26] occurs at 1556 cm^{-1}, which is significantly higher. Also found by Kim and Gewirth was a peak at 820 cm^{-1}, which they attributed to a Au–OH bending mode. Finally, no evidence was obtained for the presence of HO_2^-(ads), as no features could be discerned in their in situ SERS spectra of 10 mM H_2O_2 solutions in 0.1 M NaOH over the range 750–900 cm^{-1}. However, these authors did observe a peak at 1135 cm^{-1}, which, although a bit lower than that found in O_2-purged solutions, is still within the region associated with O_2^-.

More recently, Yu et al.[27] reported in situ SERS spectra (λ_{exc} = 785 nm) collected during the ORR on Au(poly) in acidic (0.1 M $HClO_4$), neutral (0.1 M $NaClO_4$), and basic (0.1 M KOH) aqueous solutions. In all cases, the spectra displayed two rather broad bands centered at $\tilde{\nu}$ = 1130 cm^{-1} (peak 1) and 855 cm^{-1} (peak 2) ascribed, respectively, to the O–O stretching mode of O_2^- and the O–O stretching mode of H_2O_2. In agreement with the findings of Kim and Gewirth, a clear increase in A_{int} for peak 1 was observed as E was scanned from the onset of the ORR toward negative values in basic solutions. However, and, in contrast to the earlier data, A_{int}(peak 1) reached a plateau for −0.02 V > E > −0.22 V vs SHE. Peak 2, on the other hand, was very close to that reported earlier by Li and Gewirth[28] (λ_{exc} = 668 nm, $\tilde{\nu}$ = 840 cm^{-1}) on Au(poly) in 0.1 M $HClO_4$ containing 10 mM H_2O_2. However, the latter authors failed to observe any bands in the

https://doi.org/10.1021/acs.jpcc.1c02683
J. Phys. Chem. C 2021, 125, 13862–13870

region $\tilde{\nu}$ = 750 and 900 cm^{-1} in 0.1 M NaOH containing 10 mM H_2O_2. On this basis, and as pointed out by Kim and Gewirth, the 820−840 cm^{-1} band cannot be attributed to HO_2^-(ads).

Later, Ohta et al.[29] reported the presence of two distinct features in the in situ (PD) SEIRAS (E_{ref} = 1.13 V vs SHE) of Au(poly) films supported on a semicylindrical Si prism in O_2-saturated 0.5 M $HClO_4$ at 1540 cm^{-1} (downward, broad) and 1220 cm^{-1} (upward, sharp), which they attributed, respectively, to very weakly bound O_2 and to adsorbed superoxo bound to the Au surface in an end-on configuration. The first of these features displayed a relatively large A_{int} at potentials, E, positive to the onset of O_2 reduction, E_{onset}, which decreased as E was scanned in the negative direction. In contrast, A_{int} for the second feature, was negligible for $E > E_{onset}$ and increased monotonically as E was shifted negatively. The quantitative analysis of the spectral features presented by these authors, however, may be regarded as somewhat uncertain, due primarily to the presence of additional bands in the (PD) SEIRAS spectra, which included positive- and negative-pointing bands ascribed, respectively, to one of the modes of water close to 1540 cm^{-1} and to perchlorate close to 1220 cm^{-1}, which in combination yield bipolar features. Furthermore, a detailed examination of (PD) SEIRAS spectra recorded in Ar-purged solution also revealed the presence of a weak, but definitely clear feature at 1540 cm^{-1}. More recently, Jusys and Behm[30] reported (PD) ATR-Fourier transform infrared (FTIR) spectra under forced convection in both acidic and basic electrolytes and detected what appeared to be a very weak band at 1220 cm^{-1} in 1.0 M $HClO_4$ (E_{ref} = 0.6 vs SHE in O_2-free solutions). Unfortunately, this band could not be clearly identified in otherwise identical measurements in 1 M NaOH due to the presence of a very large feature found close to 1200 cm^{-1} assigned in earlier work to a Si−O stretching mode.[31]

The experimentally observed potential dependence of A_{int} for the $\tilde{\nu}$ = 1130−1150 cm^{-1} band, assigned to O_2^-(ads), seems at odds with information obtained from other spectroscopic and electrochemical measurements. In particular, in situ SERS spectra collected for roughened Au electrodes in deaerated 1 M KOH solutions by Desilvestro and Weaver[32] (λ_{exc} = 647.1 nm) showed that the peak at ca. 400 cm^{-1}, attributed by these authors to OH^-(ads), shrinks as E decreases and virtually disappears for E < 0.044 V vs SHE. On this basis, it seems highly unlikely that a partially anionic species such as O_2^-(ads) would remain adsorbed on the Au surface and even increase in coverage at 0.4 V more negative than full OH^- desorption, as shown by Kim and Gewirth,[24] or reach a plateau for E < −0.02 V vs SHE, as found by Yu et al.[27] This argument is further reinforced by the fact that the surface concentration of O_2^- during the ORR cannot exceed the saturation concentration of O_2 by much, i.e., ca. 1.2 mM, which is nearly 3 orders of magnitude smaller than the hydroxyl concentration in 1 M KOH. Moreover, the presence of O_2^-(ads) at potentials where the current reaches diffusion-limited values for the 2 e^- ORR, $i_{Levich,2e^-}$, as reported by Kim and Gewirth,[24] and Yu et al.[27] is very difficult to rationalize, and, as such, its possible involvement as an intermediate in the ORR would seem very unlikely. It should be stressed, however, that although the existence of this spectral feature is not in question, the current spectroscopy literature for the ORR on Au provides what we interpret as being false-positive results for O_2^-(ads) and HO_2^-(ads) intermediates. This does not mean that these species are not present, only that the spectroscopy experiments fail to afford compelling evidence for their involvement; hence, mechanisms with no adsorption and with adsorption are both viable.

CONCLUDING REMARKS

Rotating ring-disk techniques have been employed to examine the kinetics of the oxygen reduction reaction, ORR, on Au(poly) in 0.1 M NaOH + 0.9 M $NaClO_4$ aqueous electrolytes containing oxygen in one case and peroxide in the other. The results obtained were found to be consistent with a mechanism proposed by Ignaczak et al.,[7] which assumes an initial outer-sphere one-electron transfer, as the rate-determining step to yield solution-phase superoxide, O_2^-(aq), which then undergoes a subsequent, fast, outer-sphere one-electron transfer, generating solution-phase peroxide, HO_2^-(aq). The results obtained were also found to be consistent with a mechanism in which O_2^-(aq) and HO_2^-(aq) were assumed to be in fast equilibrium with their corresponding adsorbed counterparts; however, a critical assessment of in situ vibrational spectroscopy data published in the literature raised questions regarding the assignment of the spectral features observed to O_2^-(ads) and HO_2^-(ads).

APPENDIX A

Zurilla et al.[4] assumed that the rate of oxidation of peroxide was of mth order in the concentration of solution-phase peroxide, $[HO_2^-]_o$,i.e.,

$$i = k[HO_2^-]_o^m \tag{A1}$$

where k is the kinetic rate constant and the subscript o (in their notation) refers to the region immediate adjacent to the electrode surface. As pointed by these authors, eq A1 would be valid for data collected at sufficiently positive potentials so that the reverse reaction, O_2 reduction to HO_2^-, could be neglected. According to fundamentals of the rotating disk electrode, for a fixed ω, $[HO_2^-]_o$, can be expressed in terms of the diffusion-limited current, i_d, and the concentration of peroxide in the bulk, $[HO_2^-]_B$, namely

$$[HO_2^-]_o = [HO_2^-]_B \frac{(i_d - i)}{i_d} \tag{A2}$$

Although not explicitly stated by these authors, eq A2 assumes a negligible contribution to the current due to HO_2^-(aq) reduction, an assertion that must be independently verified. Replacement of eq A2 into eq A1, followed by simple algebraic manipulations, may be shown to yield

$$\log i = \log k + m[HO_2^-]_B + m \log[(i_d - i)/i_d] \tag{A3}$$

On this basis, a plot of $\log i$ vs $\log[(i_d - i)/i_d]$ should yield a straight line for which the slope would be m, the reaction order. Such behavior was indeed found by Zurilla et al.[4] for Au(poly) in 0.1 M NaOH, based on polarization curves recorded in 13.4 mM H_2O_2 in 0.1 M NaOH at various rotation rates (see Figure 6 in ref 4), which reportedly yielded values of m of 0.55 for E = 1.0 and 0.95 V, and m = 1 for E = 0.90 V vs H|β-Pd (see Figure 7 in ref 4). We have digitized their dynamic polarization curves data and found the aforementioned plots to be linear; however, except for the data reported for E = 0.95 V, for which the slope was indeed ca. 0.5, and, thus, in agreement with their claim, the data for E = 1.0 V yielded a best-fit value for m of 0.36 (see panel A, Figure A1). This same overall tactic

https://doi.org/10.1021/acs.jpcc.1c02683
J. Phys. Chem. C 2021, 125, 13862−13870

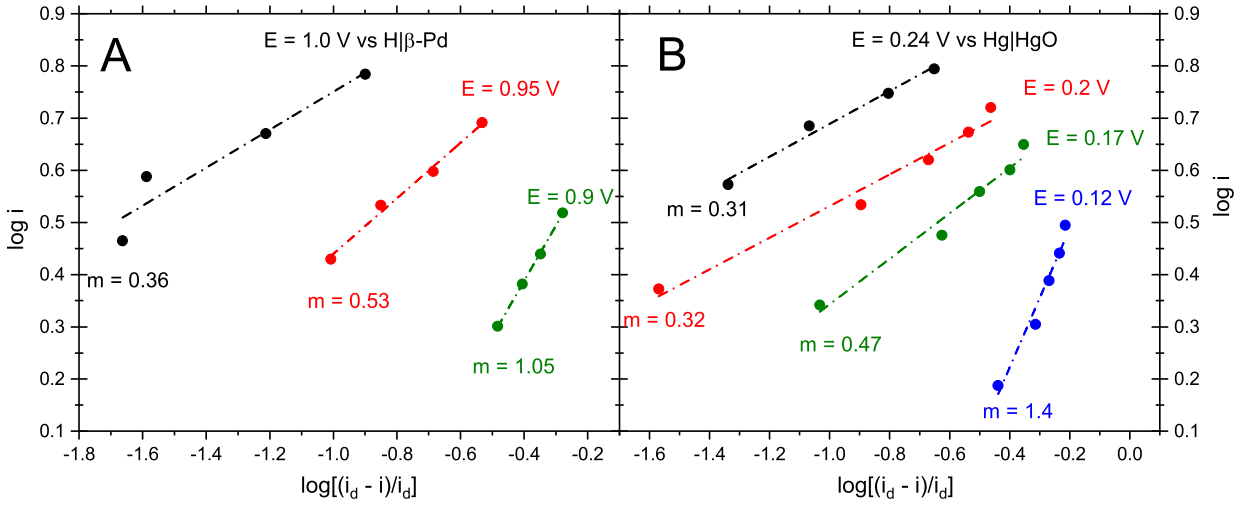

Figure A1. Plots of log i vs log$[(i_d - i)/i_d]$ based on dynamic polarization data reported by Zurilla et al.[4] for Au(poly) in 13.4 mM H_2O_2 in 0.1 M NaOH (A), and that reported by Adzić et al.[5] for Au(100) in 8.5 mM H_2O_2 in 0.1 M NaOH (B) for various values of E as specified. The corresponding linear fits are shown in dot-dash lines.

was employed by Adzić et al.[5] for the analysis of similar data collected for Au(100) in 8.5 mM H_2O_2 in 0.1 M NaOH (panel B). Surprisingly, the values we obtained based on their data (see Figure 7 in ref 5) yielded slopes of ca. 0.32 and 0.31 for E = 0.20 and E = 0.24 V vs Hg|HgO, OH^-, respectively (see panel B, Figure A1), and not 0.5 as reported by these authors (see Figure 10 in ref 5). From an overall perspective, this method can become unreliable for currents too close to the limiting current, as any small errors in $i_d - i$ can cause corresponding large errors in log$[(i_d - i)/i_d]$; in other words, the currents are essentially mass transport-controlled in this regime and, as such, afford no kinetic information.

APPENDIX B

The bulk concentration of oxygen, $[O_2]_B$, can be calculated from the ring and disk currents, i_{ring} and i_{disk}, respectively, at E_{disk} = −0.2 V, in an O_2-containing solution (see Table 1), assuming that all incoming O_2 is reduced fully to OH^-, or partway to HO_2^-(aq). Specifically, at potentials far negative to the onset of HO_2^-(aq) oxidation, k_{-12} can be neglected; hence, from the mass balance equation (Table 1), the expression for the concentration of O_2 in solution in the immediate neighborhood of the electrode, $[O_2]_{S,O_2}$, may be shown to be given by

$$[O_2]_{S,O_2} = \frac{[O_2]_B D_{O_2}/\delta_{O_2}}{k_{12} + k_3 + D_{O_2}/\delta_{O_2}} \tag{B1}$$

which can then be substituted into the expression for i_{disk,O_2} and mass balance of HO_2^-(aq) found in Table 1

$$i_{disk,O_2,E=-0.2\ V} = 2FA\left\{-k_4[HO_2^-]_{S,O_2} - \frac{(2k_3 + k_{12})[O_2]_B D_{O_2}/\delta_{O_2}}{k_{12} + k_3 + D_{O_2}/\delta_{O_2}}\right\} \tag{B2}$$

$$0 = -\frac{D_{HO_2^-}[HO_2^-]_{S,O_2}}{\delta_{HO_2^-}} + \frac{k_{12}[O_2]_B D_{O_2}/\delta_{O_2}}{k_{12} + k_3 + D_{O_2}/\delta_{O_2}} - k_4[HO_2^-]_{S,O_2} \tag{B3}$$

Furthermore, for extremely negative potentials, we can assume that $k_{12} + k_3 \gg \frac{D_{O_2}}{\delta_{O_2}}$, essentially imposing the condition that O_2 reduction takes place at near mass transport-limited rates. On this basis, eqs B2 and B3 simplify to

$$i_{disk,O_2,E=-0.2\ V} = 2FA\left\{-k_4[HO_2^-]_{S,O_2} - \frac{(2k_3 + k_{12})D_{O_2}[O_2]_B}{(k_{12} + k_3)\delta_{O_2}}\right\} \tag{B4}$$

$$0 = -\frac{D_{HO_2^-}[HO_2^-]_{S,O_2}}{\delta_{HO_2^-}} + \frac{k_{12}D_{O_2}}{\delta_{O_2}(k_{12} + k_3)}[O_2]_B - k_4[HO_2^-]_{S,O_2} \tag{B5}$$

An explicit expression for k_4 can be easily obtained by rearranging eq B5

$$k_4 = -\frac{D_{HO_2^-}}{\delta_{HO_2^-}} + \frac{k_{12}D_{O_2}}{[HO_2^-]_{S,O_2}\delta_{O_2}(k_{12} + k_3)}[O_2]_B \tag{B6}$$

which can then by substituted in eq B4 to yield

$$i_{disk,O_2,E=-0.2\ V} = -4FA\left(\frac{D_{O_2}}{\delta_{O_2}}\right)[O_2]_B + 2FA\left(\frac{D_{HO_2^-}}{\delta_{HO_2^-}}\right)[HO_2^-]_{S,O_2} \tag{B7}$$

wherein $[HO_2^-]_{S,O_2} = \frac{i_{ring,O_2}\delta_{HO_2^-}}{2FAND_{HO_2^-}}$, from which $[O_2]_B$ can be calculated using the parameter values listed in Table 3 and i_{disk,O_2} and i_{ring,O_2} for E = −0.2 V, found in Figure 1A,C, respectively, which yields $[O_2]_B$ = 0.885 mM. $[O_2]_B$ is typically closer to 1.2 mM for 0.1 M NaOH or KOH,[33] but Mei et al. have also reported a smaller $[O_2]_B$ in mixed NaOH/$NaClO_4$ solutions.[34]

AUTHOR INFORMATION

Corresponding Author

Daniel Scherson − *Department of Chemistry, Case Western Reserve University, Cleveland, Ohio 44016-7078, United States;* orcid.org/0000-0001-6353-3021; Email: dxs16@case.edu

https://doi.org/10.1021/acs.jpcc.1c02683
J. Phys. Chem. C 2021, 125, 13862−13870

Author

Jonathan R. Strobl − *Department of Chemistry, Case Western Reserve University, Cleveland, Ohio 44016-7078, United States;* orcid.org/0000-0003-4796-3587

Complete contact information is available at: https://pubs.acs.org/10.1021/acs.jpcc.1c02683

Notes

The authors declare no competing financial interest.

■ ACKNOWLEDGMENTS

Support for this work was provided by NSF, CHE-1808592 and CHE-1412060. The authors express their appreciation to Arvind Singh Heer for the careful digitization of the literature data in Appendix A and to Prof. Christian Amatore for enlightening discussions.

■ REFERENCES

(1) Markovic, N. M.; Schmidt, T. J.; Stamenkovic, V.; Ross, P. N. Oxygen Reduction Reaction on Pt and Pt Bimetallic Surfaces: A Selective Review. *Fuel Cells* **2001**, *1*, 105−116.

(2) Ge, X.; Sumboja, A.; Wuu, D.; An, T.; Li, B.; Goh, T.; Hor, T. S. A.; Zong, Y.; Liu, Z. Oxygen Reduction in Alkaline Media: From Mechanisms to Recent Advances of Catalysts. *ACS Catal.* **2015**, *5*, 4643−4667.

(3) Wang, Y.; Li, J.; Wei, Z. Recent Progress of Carbon Based Materials in Oxygen Reduction Catalysis. *ChemElectroChem* **2018**, *5*, 1764−1774.

(4) Zurilla, R. W.; Sen, R. K.; Yeager, E. The Kinetics of the Oxygen Reduction Reaction on Gold in Alkaline Solution. *J. Electrochem. Soc.* **1978**, *125*, 1103−1109.

(5) Adzić, R. R.; Marković, N. M.; Vešović, V. B. Structural Effects in Electrocatalysis Oxygen Reduction on the Au(100) Single Crystal Electrode. *J. Electroanal. Chem. Interfacial Electrochem.* **1984**, *165*, 105−120.

(6) Anastasijević, N. A.; Vesovic, V.; Adzić, R. R. Determination of the Kinetic Parameters of the Oxygen Reduction Reaction Using the Rotating Ring-Disk Electrode Part I. Theory. *J. Electroanal. Chem. Interfacial Electrochem.* **1987**, *229*, 305−316.

(7) Ignaczak, A.; Nazmutdinov, R.; Goduljan, A.; Moreiro de Campos Pinto, L.; Juarez, F.; Quaino, P.; Santos, E.; Schmickler, W. A scenario for oxygen reduction in alkaline media. *Nano Energy* **2016**, *26*, 558−564.

(8) Gong, S.; Lu, J.; Yan, H. Developing the self-contained hydrogen reference electrode. *J. Electroanal. Chem.* **1997**, *436*, 291−293.

(9) Strobl, J. R.; Georgescu, N. S.; Scherson, D. Solution phase superoxide as an intermediate in the oxygen reduction reaction on glassy carbon in alkaline media. *Electrochim. Acta* **2020**, *335*, No. 135432.

(10) Feng, Z.; Georgescu, N. S.; Scherson, D. A. Rotating Ring-Disk Electrode Method for the Detection of Solution Phase Superoxide as a Reaction Intermediate of Oxygen Reduction in Neutral Aqueous Solutions. *Anal. Chem.* **2016**, *88*, 1088−1091.

(11) Bard, A. J.; Faulkner, L. R. Multistep Mechanisms. In *Electrochemical Methods Fundamentals and Applications*, 2nd ed.; Harris, D., Ed.; John Wiley & Sons, Inc.: New York, 2001; pp 107−115.

(12) Harris, D. C. Biochemists Use E°'. In *Quantitative Chemical Analysis*, 8th ed.; Fiorillo, J., Ed.; W. H. Freeman and Co.: New York, 2010; pp 297−301.

(13) Wood, P. M. The Redox Potential of the System Oxygen-Superoxide. *FEBS Lett.* **1974**, *44*, 22−24.

(14) Wood, P. M. The two redox potentials for oxygen reduction to superoxide. *Trends Biochem. Sci.* **1987**, *12*, 250−251.

(15) Electrochemical Series. In *CRC Handbook of Chemistry and Physics*; 101st ed.; Rumble, J. R., Ed.; CRC Press/Taylor & Francis: Boca Raton, FL, 2020.

(16) Activity Coefficients of Acids, Bases and Salts at 25 °C. In *CRC Handbook of Chemistry and Physics*, 101st ed.; Rumble, J. R., Ed.; CRC Press/Taylor & Francis: Boca Raton, FL, 2020.

(17) Srejić, I.; Smiljanić, M.; Rakočević, Z.; Štrbac, S. Oxygen Reduction on Au(100)-like Polycrystalline Gold Electrode in Alkaline Solution. *Int. J. Electrochem. Sci.* **2016**, *11*, 10436−10448.

(18) Paliteiro, C. (100)-Type Behaviour of Polycrystalline Gold Towards O2 Reduction. *Electrochim. Acta* **1994**, *39*, 1633−1639.

(19) Wroblowa, H. S.; Pan, Y.-C.; Razumney, G. Electroreduction of Oxygen A New Mechanistic Criterion. *J. Electroanal. Chem. Interfacial Electrochem.* **1976**, *69*, 195−201.

(20) Hernández, J.; Solla-Gullon, J.; Herrero, E.; Feliu, J. M.; Aldaz, A. In Situ Surface Characterization and Oxygen Reduction Reaction on Shape-Controlled Gold Nanoparticles. *J. Nanosci. Nanotechnol.* **2009**, *9*, 2256−2273.

(21) Prieto, A.; Hernandez, J.; Herrero, E.; Feliu, J. M. The role of anions in oxygen reduction in neutral and basic media on gold single-crystal electrodes. *J. Solid State Electrochem.* **2003**, *7*, 599−606.

(22) Shao, M. H.; Adzić, R. R. Spectroscopic Identification of the Reaction Intermediates in Oxygen Reduction on Gold in Alkaline Solutions. *J. Phys. Chem. B* **2005**, *109*, 16563−16566.

(23) Brooker, J.; Christensen, P. A.; Hamnett, A.; He, R.; Paliteiro, C. A. Combined Scanning Tunnelling Microscopy and in situ Fouriertransform Infrared Study of Dioxygen Reduction on Gold. *Faraday Discuss.* **1992**, *94*, 339−360.

(24) Kim, J.; Gewirth, A. A. Mechanism of Oxygen Electroreduction on Gold Surfaces in Basic Media. *J. Phys. Chem. B.* **2006**, *110*, 2565−2571.

(25) Hunter-Saphir, S. A.; Creighton, J. A. Resonance Raman Scattering from the Superoxide Anion. *J. Raman Spectrosc.* **1998**, *29*, 417−419.

(26) Weber, A.; McGinnis, E. A. The Raman Spectrum of Gaseous Oxygen. *J. Mol. Spectrosc.* **1960**, *4*, 195−200.

(27) Yu, H.-Y.; Li, X.-F.; Zhang, T.-H.; Liu, J.; Tian, J.-H.; Yang, R. Oxygen Reduction Reaction on Au Revisited at Different pH Values Using In Situ Surface-Enhanced Raman Spectroscopy. *ChemSusChem* **2020**, *13*, 2702−2708.

(28) Li, X.; Heryadi, D.; Gewirth, A. A. Electroreduction Activity of Hydrogen Peroxide on Pt and Au Electrode. *Langmuir* **2005**, *21*, 9251−9259.

(29) Ohta, N.; Nomura, K.; Yagi, I. Adsorption and Electroreduction of Oxygen on Gold in Acidic Media: In Situ Spectroscopic Identification of Adsorbed Molecular Oxygen and Hydrogen Superoxide. *J. Phys. Chem. C.* **2012**, *116*, 14390−14400.

(30) Jusys, Z.; Behm, R. J. The Effect of Anions and pH on the Activity and Selectivity of an Annealed Polycrystalline Au film Electrode in the Oxygen Reduction Reaction-Revisited. *ChemPhysChem* **2019**, *20*, 3276−3288.

(31) Philipsen, H. G. G.; Ozanam, F.; Allongue, P.; Kelly, J. J.; Chazalviel, J.-N. Oxide Formation and Dissolution on Silicon in KOH Electrolyte: An In-Situ Infrared Study. *J. Electrochem. Soc.* **2016**, *163*, H327−H338.

(32) Desilvestro, J.; Weaver, M. J. Surface Structural Changes during Oxidation of Gold Electrodes in Aqueous Media as Detected using Surface-Enhanced Raman Spectroscopy. *J. Electroanal. Chem. Interfacial Electrochem.* **1986**, *209*, 377−386.

(33) Gubbins, K. E.; Walker, R. D. The Solubility and Diffusivity of Oxygen in Electrolytic Solutions. *J. Electrochem. Soc.* **1965**, *112*, 469−471.

(34) Mei, D.; He, Z. D.; Zheng, Y. L.; Jiang, D. C.; Chen, Y.-X. Mechanistic and Kinetic Implications on the ORR on a Au(100) Electrode: pH, Temperature and H-D Kinetic Isotope Effects. *Phys. Chem. Chem. Phys.* **2014**, *16*, 13762−13773.

(35) Han, P.; Bartels, D. M. Temperature Dependence of Oxygen Diffusion in H_2O and D_2O. *J. Phys. Chem. A* **1996**, *100*, 5597−5602.

(36) Csóka, B.; Nagy, G. Determination of Diffusion Coefficient in Gel and in Aqueous Solutions using Scanning Electrochemical Microscopy. *J. Biochem. Biophys. Methods* **2004**, *61*, 57−67.